

Article

Precipitation Behavior of the Metastable Quasicrystalline *I*-Phase and θ' -Phase in Al-Cu-Mn Alloy

Anastasia V. Mikhaylovskaya ^{1,*}, Aiyngul Mukhamejanova ¹, Anton D. Kotov ¹, Nataliya Yu. Tabachkova ², Alexey S. Prosviryakov ¹ and Andrey G. Mochugovskiy ¹

¹ Physical Metallurgy of Non-Ferrous Metals, National University of Science and Technology MISiS, Leninsky Prospekt, 4, 119049 Moscow, Russia

² Prokhorov General Physics Institute of the Russian Academy of Sciences, Vavilov str. 38, 119991 Moscow, Russia

* Correspondence: mihaylovskaya@misis.ru; Tel.: +7-495-6384480

Abstract: The precipitation behavior and mechanical properties for conventionally solidified Al-2.0wt.%Cu-2.0wt.%Mn alloy were studied. The supersaturated aluminum-based solid solution, CuAl₂, Al₆Mn and Al₂₀Cu₂Mn₃ phases of solidification origin were identified after casting. The high temperature ageing of as-cast samples (T5 treatment) in a temperature range of 300–350 °C led to the formation of the metastable θ' phase and equiaxed precipitates of the quasicrystalline-structured *I*-phase. The θ' phase demonstrated a high size stability in a studied temperature range with a mean length of ~300 nm and a mean thickness of ~24 nm. A mean size of the *I*-phase precipitates varied in a range of ~30–50 nm depending on the treatment regimes. The rod-shaped *T*-phase precipitates were formed with an increase in ageing temperature to 400 °C. Mechanical properties were analyzed at room temperature in a solid solution-treated state. The increased yield strength at room temperature and 200–300 °C were observed after ageing at 300 °C for 148 h.

Keywords: aluminum alloys; precipitates; aging; mechanical properties



Citation: Mikhaylovskaya, A.V.; Mukhamejanova, A.; Kotov, A.D.; Tabachkova, N.Y.; Prosviryakov, A.S.; Mochugovskiy, A.G. Precipitation Behavior of the Metastable Quasicrystalline *I*-Phase and θ' -Phase in Al-Cu-Mn Alloy. *Metals* **2023**, *13*, 469. <https://doi.org/10.3390/met13030469>

Academic Editors: Ramakanta Naik and Anna H. Kaksonen

Received: 20 December 2022

Revised: 30 January 2023

Accepted: 20 February 2023

Published: 24 February 2023



Copyright: © 2023 by the authors. Licensee MDPI, Basel, Switzerland. This article is an open access article distributed under the terms and conditions of the Creative Commons Attribution (CC BY) license (<https://creativecommons.org/licenses/by/4.0/>).

1. Introduction

Aluminum-based alloys exhibit low density and good mechanical properties at room temperature but limited high temperature strength above 200–250 °C. The promising aluminum-based alloys for high temperature application are based on Al-Cu-Mn-(Zr) system with the main strengthening phases of θ' and *T*-Al₂₀Cu₂Mn₃ [1–10]. To increase the high temperature strength and creep resistance, a high fraction of fine and thermally stable precipitates are required. The precipitates parameters depend on temperature and time of ageing, and alloy's composition. The θ' -phase is formed during low temperature ageing after solid solution treatment and exhibits a low thermal stability at service temperatures of 250–300 °C. The Mn, Zr, Sc segregations to the θ' interphases increase coarsening resistance of the θ' -phase precipitates [11–14] and improve high temperature properties of the alloys. The precipitation behavior and mechanical properties of the alloys with high Cu/Mn ratio are well studied [15–17]. Meanwhile, the alloys with a low Cu and an increased Mn are also promising and their microstructure and properties require further investigation. The Mn-enriched phases, which are precipitated at high temperature ageing, exhibit superior thermal stability compared to that for the θ' -phase. The supersaturated by Mn solid solution is formed during solidification and the orthorhombic *T*-phase is precipitated at temperatures above 400 °C during ageing of as-cast alloys [1–3,18–20]. Heat treatment of the Mn-supersaturated solid solution in a temperature range of 300–400 °C provides fine precipitates of the quasicrystalline icosahedral *I*-phase and decagonal *D*-phase formed in Mn-bearing alloys [21–29]. In Al-(2–4)%Mn-(2–4)%Cu-(0.3–0.7)%Be alloys, a high number density of the *I*-phase precipitates was formed after annealing at 300 °C for 24–168 h [21,22,30]. The size of spheroidal *I*-phase precipitates is 10–20 nm that proposed a

high strengthening effect [31,32]. At temperatures of 400 °C and short ageing time for 1 h, the *I*-phase precipitates have grown and, in addition, quasicrystalline decagonal *D*-phase is formed. At higher temperatures above 450 °C, coarser particles of the orthorhombic *T*-phase are precipitated [21,33].

Quasicrystalline phases usually have a solidification origin [34–38] and Be [39,40], and co-addition of Ca, Sr, and Zn [41] stimulates the quasicrystalline phases formation during solidification. Authors of [42] also suggest that Be has an impact to the formation of the quasicrystalline phases during heat treatment. Due to a nanoscale size and an equiaxed shape at ageing temperatures of 300–350 °C, the quasicrystalline phases precipitated during solid solution decomposition have a high practical importance. Be-free conventional Al-Cu-Mn alloys are usually heat-treated at high temperatures, above 400 °C, where *T*-phase is formed, and the precipitation behavior is poorly studied at lower temperatures, where quasicrystalline phases and fine Mn-bearing precipitates are possible. The present study focuses on the analysis of the precipitation behavior in a range of 300–400 °C with detailed microstructural investigations of the precipitates type and size for Al-2%Cu-2%Mn alloy to identify heat treatment parameters providing fine precipitates of the *I*-phase.

2. Materials and Methods

The Al-2%Cu-2%Mn (wt.%) alloy was prepared in an Interselt induction furnace in a graphite chamotte crucibles. Pure Al (99.99%), Al-53.5%Cu, and Al-10%Mn master alloys were used for alloy preparation. The increased cooling rate of ~15 K/s during solidification was reached by casting in a water-cooling copper mold. The cast samples were heat-treated in air-circulation furnace Nabertherm N 30/65A followed by water quenching to room temperature. The heat treatment temperature was in a range of 300–450 °C and time was varied from 0.5 to 200 h. The X-ray diffraction (XRD) analysis was carried out using a Bruker D8 Advanced diffractometer at a Cu-K α radiation.

The dependences of Vickers hardness (HV) vs. annealing time were obtained through the annealing at 300 °C, 350 °C, 400 °C, and 450 °C. The Wolpert DigiTestor 930/250 N was used to measure Vickers hardness. The measurements were performed at a load of 5 kg, load application time of 15 s, by averaging from ten to twenty values. The error bars were calculated as a confidence interval for a confidence probability of 0.95.

The in situ evolution of electrical resistance (ρ) was measured during annealing at 300 °C, 325 °C, 450 °C up to 200 h. Measurements were performed in electrical resistance furnace by INSTEK GOM-802 milliohm meter GOM-802, using the samples with size of $1.5 \times 1.5 \times 70 \text{ mm}^3$.

Microstructures of as-cast and heat-treated specimens were studied by scanning and transmission electron microscopy (SEM and TEM). SEM was performed in a Tescan-VEGA3 LMH microscope equipped with energy-dispersive X-ray spectrometer (EDS) X-MAX80, Oxford Instruments. TEM was performed using a JEOL JEM 2100 microscope at an operating voltage of 200 kV. The samples for SEM studies were prepared by mechanical grinding and polishing using a Struers LaboPol-5 machine. The samples for TEM studies were thinned by mechanical grinding to $0.25 \pm 0.02 \text{ mm}$ and subsequent electric polishing in a solution of 30% HNO₃ and 70% methanol using a Struers TenuPol-5 machine.

A mean size and volume fraction of precipitates of solidification-originated phases were measured by a linear secant method for five-six SEM micrographs at 1000–3000 magnification. A mean diameter for near-equiaxed shape secondary precipitates and both longitudinal and cross sizes for elongated precipitates were measured in TEM micrographs. The mean size was calculated by averaging of at least 160 measurements. The error bars were calculated using a standard deviation and a confidence probability of 0.95.

The as-cast specimens for compression test with dimensions of $5 \times 5 \times 8 \text{ mm}^3$ were prepared using a spark-erosion-cutting machine and subjected to heat treatment according to regimes indicated in Table 1. The compression tests were carried out using a Zwick-Z25

universal testing machine at 20, 200 and 300 °C with a total strain of 0.5 and an initial strain rate of 10^{-3} s^{-1} . Three samples per point were tested.

Table 1. Yield strength (MPa) at different compression temperatures of the alloys studied after aging of as-cast alloy (error bars are the standard deviation of a mean value).

Aging Regime	Compression Test Temperature		
	20 °C *	200 °C **	300 °C **
450 °C, 4 h	85 ± 3	80 ± 2	51 ± 2
400 °C, 32 h	100 ± 3	92 ± 3	53 ± 2
350 °C, 48 h	96 ± 4	91 ± 3	57 ± 1
300 °C, 148 h	97 ± 3	94 ± 2	62 ± 1

* water-quenched state; ** water-quenching from the aging temperature and second step stabilizing treatment at 300 °C for 1 h.

3. Results

The XRD data for as-cast sample (Figure 1) suggested the solidification of the aluminum-based solid solution (Al) and several secondary phases of CuAl_2 , $\text{Al}_{20}\text{Cu}_2\text{Mn}_3$, and Al_6Mn . Owing to a small fraction of the secondary phases in the studied alloy, the precise identification of the secondary phases by XRD method was difficult and microstructural investigations was involved. Meanwhile, the suggested phases are agreed to Al-Cu-Mn phase diagram [43] and Thermo-Calc simulation [18].

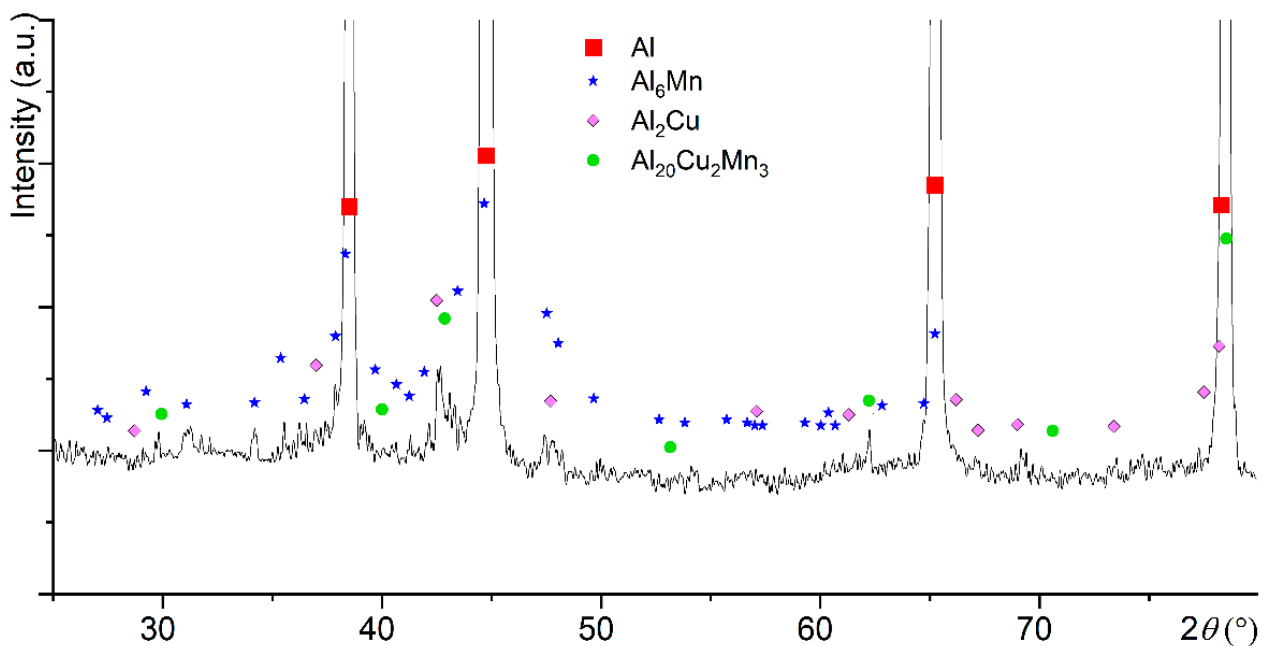


Figure 1. XRD data for the Al-2%Cu-2%Mn as-cast alloy studied (Cu K- α radiation).

In the SEM structure of as-cast alloy, the grey-colored aluminum solid solution matrix phase and bright areas of constitutes phases enriched with Cu, Mn, and both Mn and Cu were observed (Figure 2). The morphology of the secondary phases and EDS data suggested that the bright areas belonged to solidification-originated θ - Al_2Cu , Al_6Mn , and T - $\text{Al}_{20}\text{Cu}_2\text{Mn}_3$ phases. The total volume fractions of the secondary phases was $1.8 \pm 0.2\%$, with $1.0 \pm 0.1\%$ of θ - Al_2Cu phase. According to SEM-EDS data, the (Al) solid solution contained $1.7 \pm 0.2 \text{ wt.}\%$ Mn and $1.2 \pm 0.3 \text{ wt.}\%$ Cu in as-cast state. The dendrite liquation of Cu, which enriched periphery of dendrite cells, was observed. The phase composition of

the studied alloy is typical for Al-Cu-Mn-based alloys [1,44]. The Thermo-Calc calculations suggested that two main phases of (Al) and $T\text{-Al}_{20}\text{Cu}_2\text{Mn}_3$ should be observed after equilibrium solidification, and $\theta\text{-Al}_2\text{Cu}$ and Al_6Mn are non-equilibrium phases [1].

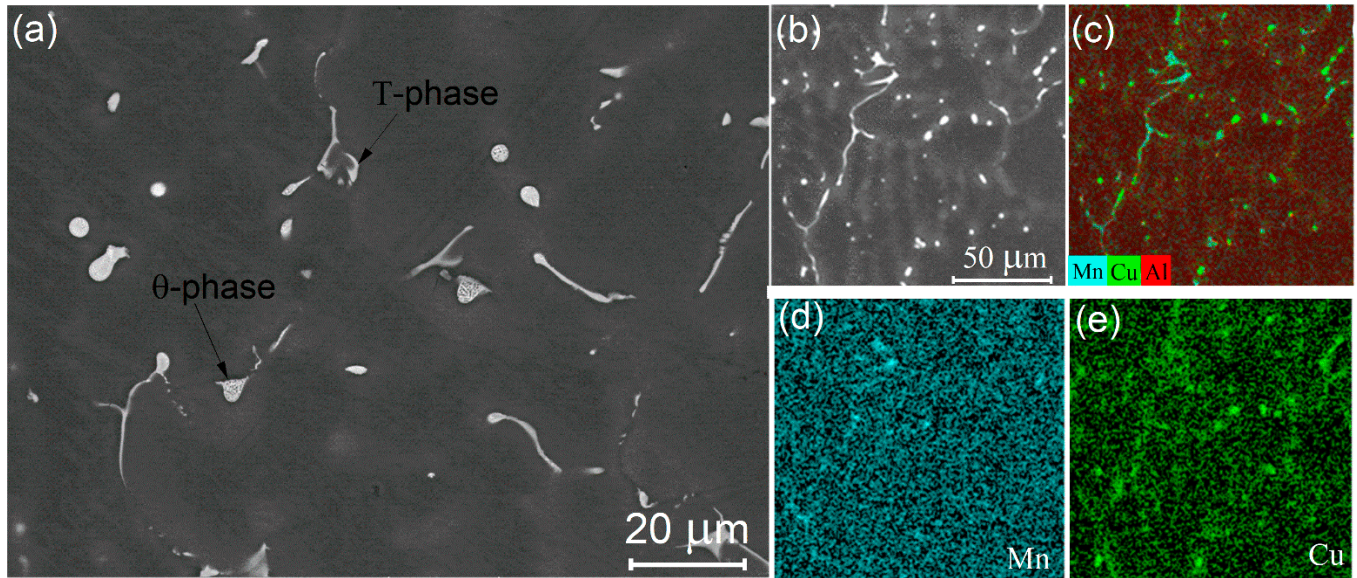


Figure 2. (a,b) The as-cast microstructure of the Al-2%Cu-2%Mn alloy, (c) EDS layered image, (d) Mn-distribution map, and (e) Cu distribution map for image in (b).

During aging at 300 °C the hardness slightly increased at the beginning of annealing (Figure 3a). An increase in time above 96 h led to an additional hardening effect, and hardness values stabilized after ~148 h of aging. Heat treatment at 350 °C led to hardening in a range of 8–48 h and stabilization of HV values at larger time. After aging at higher temperature of 400 °C, HV-time curve had a maximum at 32 h. Similarly, at 450 °C, hardness grew during aging for 4 h and then decreased. The evolution of electrical resistance was studied in-situ at 300, 325, and 350 °C (Figure 3b). The electrical resistance insignificantly changed up to 7–10 h of aging and continuously decreased with a further increase of aging time.

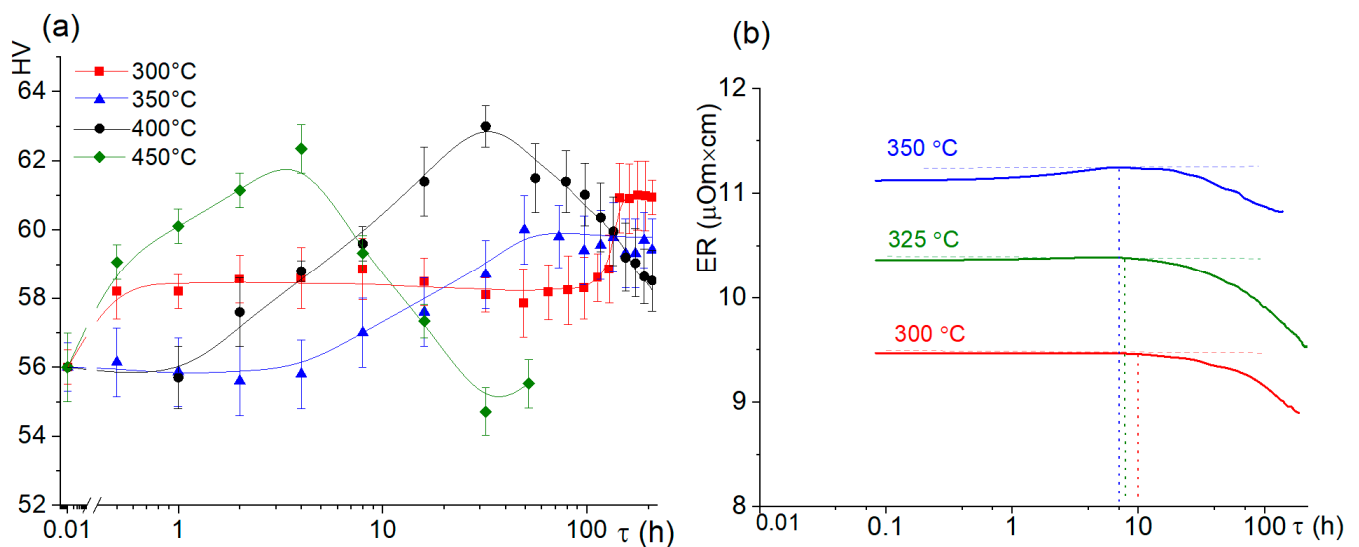


Figure 3. (a) The hardness and (b) electrical resistance evolution vs. annealing time for the as-cast Al-2%Cu-2%Mn alloy.

Several processes were expected during heat treatment of the as-cast alloy in a temperature range of 300–400 °C below the solvus point. First, the dissolution of the non-equilibrium θ -phase of solidification origin with enrichment of the solid solution with Cu at elevated temperatures, second, the precipitation of secondary metastable or stable Cu-enriched θ phase, and third, the formation of secondary precipitates of the Mn-enriched phases or both Mn- and Cu-enriched T -phase were suggested.

As it was shown by SEM study (Figure 4a,d), low temperature annealing at 300 °C for 8 h and for 148 h led to precipitation of the platelet-like metastable θ' -phase with a typical morphology on the periphery of dendrite cells, that agreed to [45–50]. The morphology of the non-equilibrium θ -CuAl₂ particles did not change (Figure 4a,d). With increasing annealing time from 8 to 148 h, the number density and size of the θ' -phase precipitates changed insignificantly. Similar θ' -phase precipitates was observed after treatment at 350–400 °C, but a number density of precipitates in this temperature range significantly decreased with increasing aging time (Figure 4b,c,e). Non-equilibrium θ -CuAl₂ phase dissolved and its volume fraction decreased to $\sim 0.6 \pm 0.2\%$ at 350 °C for 48 h and to $\sim 0.2 \pm 0.1\%$ at 400 °C for 32 h. In addition, fine equiaxed precipitates were observed after aging at 350–400 °C (green arrows in Figure 4e,f). TEM studies were involved for precise identification of the precipitates parameters.

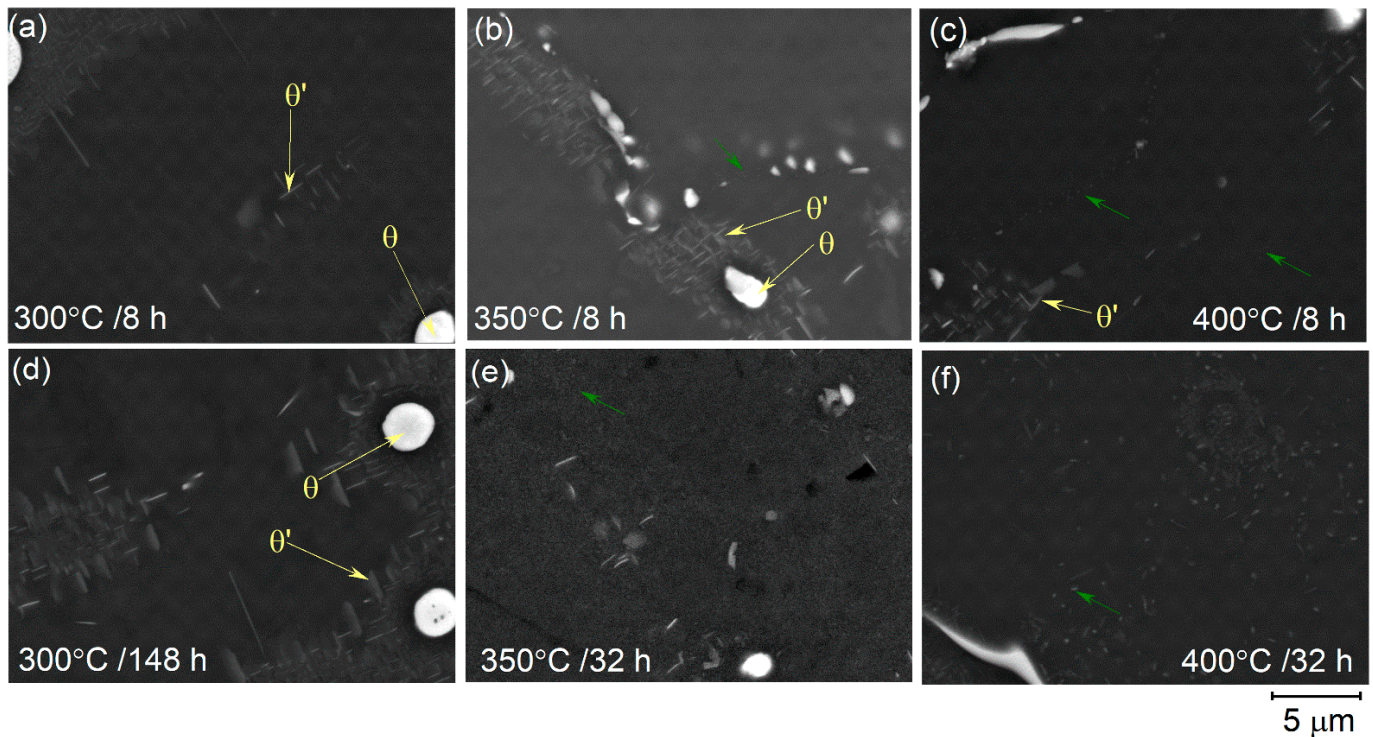


Figure 4. SEM-BSE micrographs for the Al-2%Cu-2%Mn alloy aged at (a,d) 300 °C (b,e) 350 °C (c,f) 400 °C.

After ageing at 300 °C for 8 h, the θ' -phase precipitates (Figure 5a,b) were confirmed. The mean θ' precipitates length was 290 ± 50 nm and the mean thickness of precipitates was 24 ± 5 nm. Increase ageing time to 148 h (Figure 5c–i) led to a high number density of fine I -phase precipitates but the θ' -phase precipitates parameters remained the same with a mean length of 310 ± 40 nm and a mean thickness of 23 ± 4 nm. According to [15,16] the high stability of the θ' -phase can be the result of Mn atomic segregations to the θ' interphases. A mean size of the I -phase precipitates was 35 ± 5 nm. It is notable that after similar ageing conditions, the fine I -phase dispersoids are precipitated in Al-Cu-Mn-Be alloy [21,22].

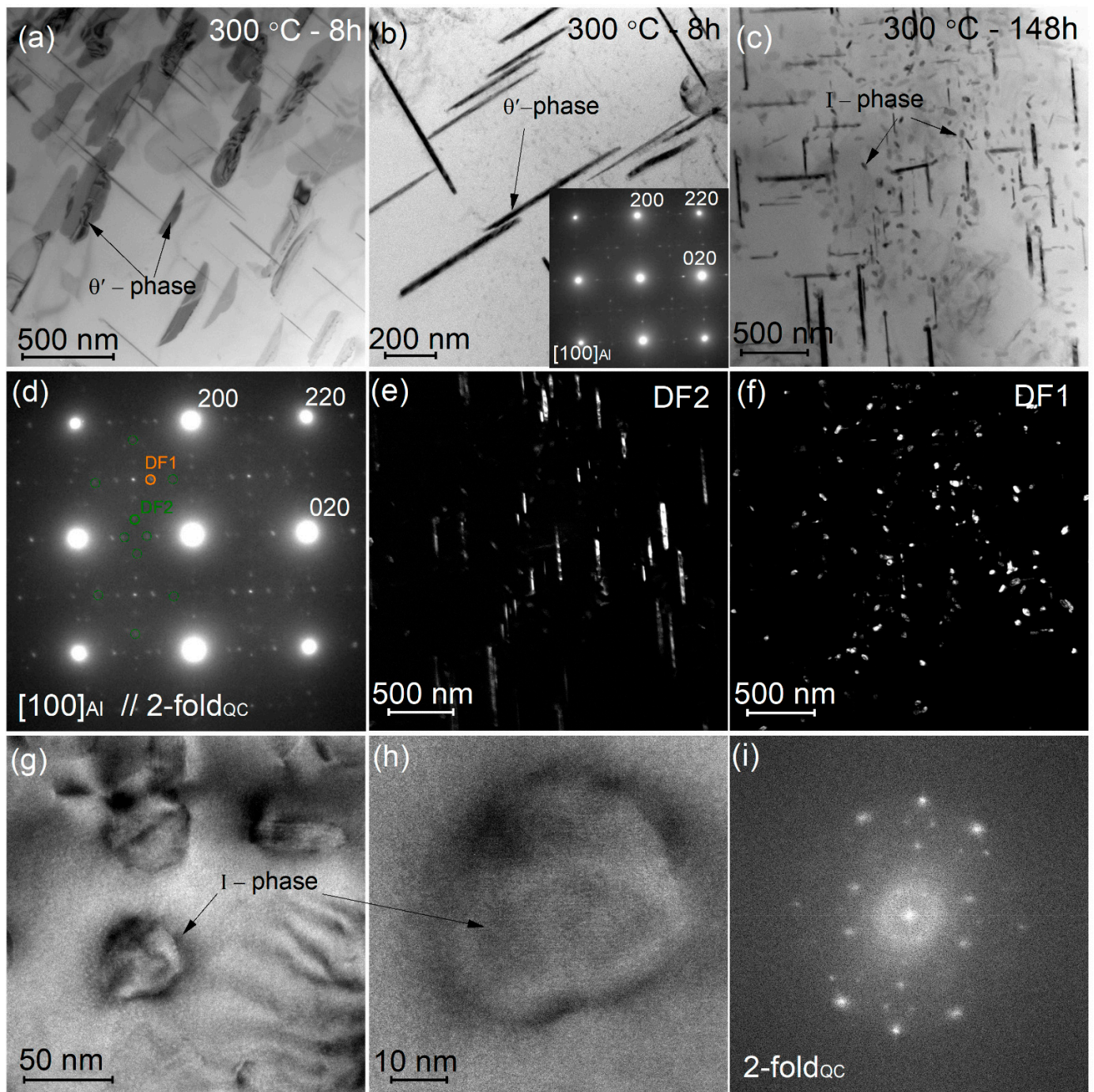


Figure 5. (a–c,e,f) TEM images and (d) SAEDs of the Al-2%Cu-2%Mn alloy subjected to aging for (a,b) 8 h and (c–i) 148 h at 300 °C; (a,b,c) bright field; (e,f) dark field; (g,h) high resolution images; and (i) FFT of high resolution images.

After annealing for 4 h, 8 h, and 48 h at 350 °C (Figure 6), both θ' -phase plates and fine near-equiaxed precipitates were observed. Fine near-equiaxed precipitates exhibited an Ashby-Brown contrast (Figure 6b,i) and a Moiré pattern (Figure 6d), which suggested coherency/semi-coherency to (Al) matrix. A Fast Fourier Transform (FFT) of the high-resolution images for most of precipitates demonstrated the pattern of two-fold symmetry of the *I*-phase (Figure 6e,f). Depending on the aging time, a mean size of near-equiaxed precipitates was $(33\text{--}38) \pm 3$ nm after annealing at 350 °C. An increase in the heat treatment time to 48 h (peak aging time) led to a higher number density of precipitates (Figure 6g,i),

but insignificantly changed their mean size and structure. Some particles belonged to the crystalline phases but the precipitates were also semi-coherent to the aluminum matrix.

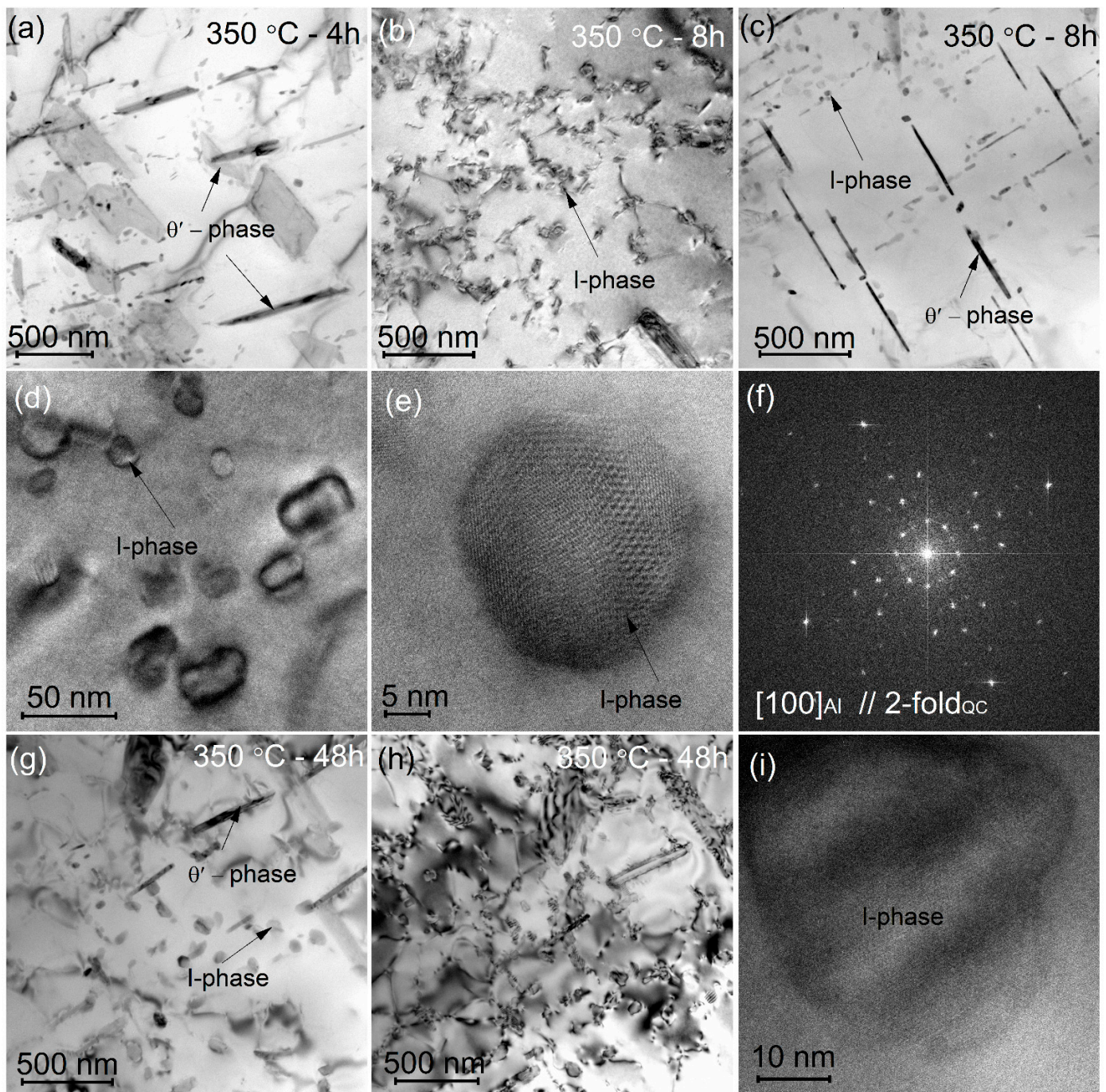


Figure 6. (a–d,g,h) Bright field TEM images of the Al-2%Cu-2%Mn alloy subjected to aging for (a) 4 h, (b–f) 8 h, and (g–i) 48 h at 350 °C; (e,i) high-resolution images; (f) FFT of high resolution image (e).

Heat treatment at 400 °C for 3 h led to a high number density of precipitates with a size in a range of 41 nm to 120 nm, respectively (Figure 7). The diffraction pattern after 3 h of annealing revealed reflexes belonged to the θ' -phase and some extra-reflexes suggested precipitation of an additional crystalline phase (see SAED in Figure 7d). The θ' phase was not found, and predominantly rod-shaped precipitates of the T -phase were observed after peak aging for 32 h (SAEDs in Figure 7e,f). The length of the T -phase precipitates

was varied in a range of 118 to 236 nm. Some precipitates exhibited hexagon shape and demonstrated ten-fold symmetry SAED (Figure 7c,f). According to [51,52], the *T*-phase is an approximant of the decagonal quasicrystal. This microstructure may be the result of multiple-twinning of the *T*-phases during its growth [53–56].

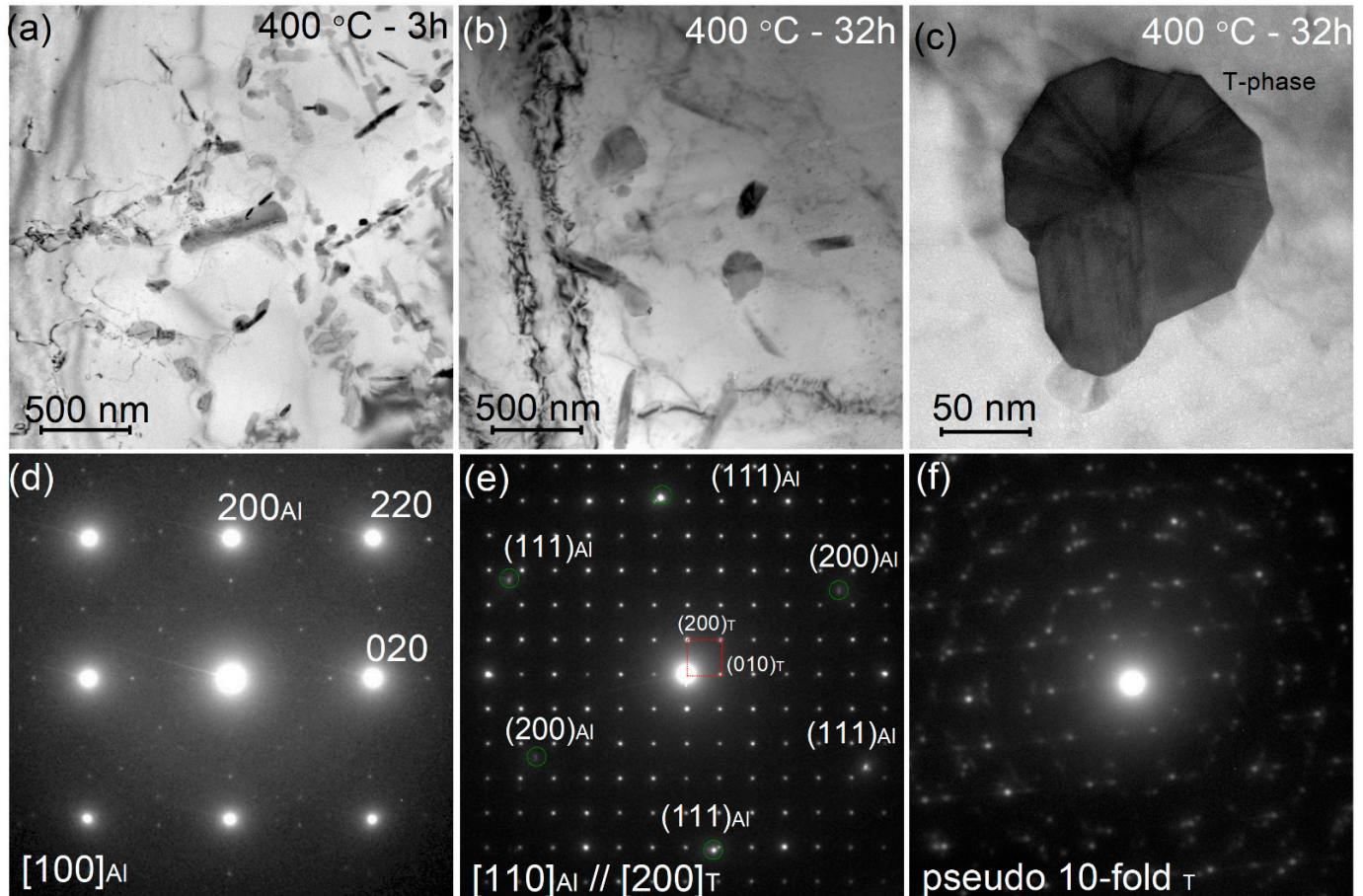


Figure 7. (a–c) Bright field TEM images and corresponded SAEDs for the Al-2%Cu-2%Mn alloy subjected to aging for (a,d) 3 h, (b,c,e,f) 32 h at 400 °C.

The evolution of hardness and electrical resistance during annealing depends on the cooperation of the several processes occurred in the microstructure of the studied alloy. The precipitation of θ' -phase at small annealing time at 300 °C leads to some hardening effect at the beginning of annealing for ~8 h. Higher annealing time led to a further hardening resulted of Mn-enriched *I*-phases precipitation. Decomposition of the solid solution with precipitation of the Mn-bearing phases also decreased in electrical resistance after annealing time above 7–10 h at 300–350 °C. Annealing at 400–450 °C provided hardening effect after smaller time that is reasonable due to potentially higher diffusivity. At these temperatures, the dissolution of the θ -phase and an increase in Cu content in solid solution with subsequent precipitation of the *T*-phase occurred.

The most promised aging regimes for T5 treatment that led to the formation of a high number density of fine precipitates are long-term aging at 300 °C (for ~148 h) or aging at 350 °C for 48 h. This aging should provide a high strengthening effect due to the Mn-enriched *I*-phase precipitation. Aging at 400 °C led to a dissolution of the θ -phase and change in the precipitates structure from the quasicrystalline to the crystalline with formation of the coarser Cu- and Mn-bearing *T*-phase precipitates.

The strength properties were determined after compression tests with initial strain rate of 10^{-3} s^{-1} at room temperature, 200 °C and 300 °C to compare the different aging regimes (Table 1). Properties at room temperature are presented in as-quenched state. All

samples for high temperature compression tests were heat-treated at 300 °C for 1 h to stabilize microstructure and properties and to avoid an effect of dynamic precipitation of the during compression tests for the samples pre-treated at higher temperatures of 400–450 °C. Engineering stress–engineering strain compression curves for 200 °C and 300 °C are presented in Figure 8. Ageing of as-cast samples at 300–400 °C provided a higher yield strength at room temperature and at 200 °C, than that of ageing at 450 °C. Notable that the difference between yield strength at room temperature and 200 °C was insignificant. The yield strength and stress level during compression at a testing temperature of 300 °C strongly decreased comparing to 200 °C, meanwhile, the values increased by 20% with a decrease in aging temperature from 450 to 300 °C (at a time corresponded to the peak hardness).

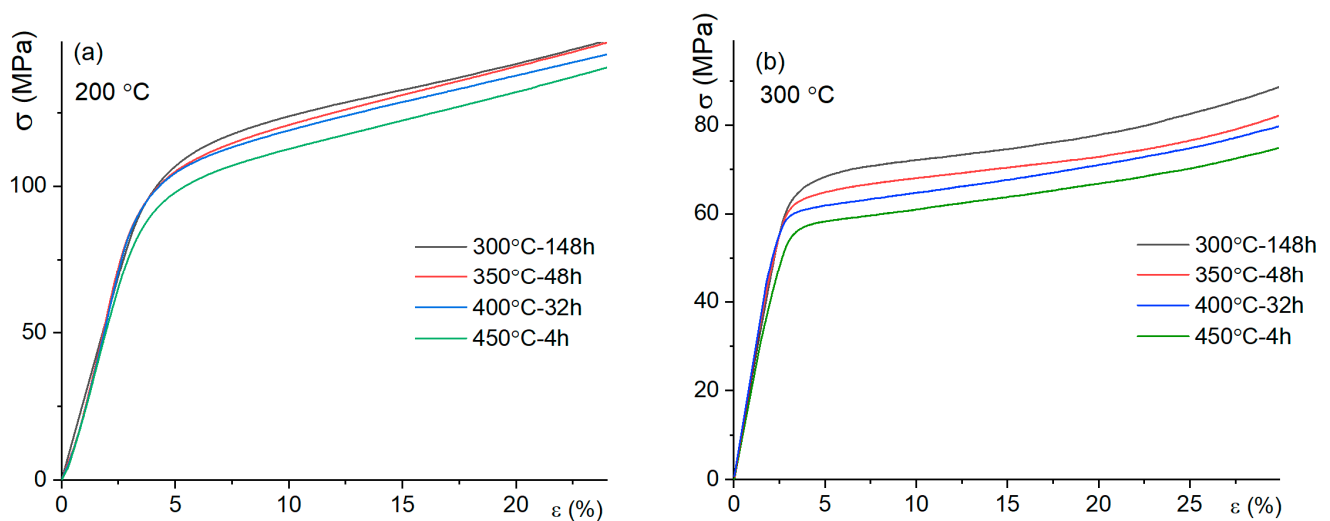


Figure 8. (a,b) Engineering stress–engineering strain compression curves at temperatures of (a) 200 °C and (b) 300 °C for the Al-2%Cu-2%Mn alloy heat-treated with different ageing regimes and final stabilizing aging at 300 °C to 1 h.

The strength properties for the studied alloy depend on precipitation strengthening and solid solution strengthening effects. Cu solute content increased with an increase in aging temperature and led to a higher solid solution strengthening effect and higher precipitation strengthening effect. The predicted by Thermo-Calc equilibrium Cu content in the (Al) solid solution increased insignificantly from 0.47 wt.% (0.2 at%) at 300 °C to 0.65 wt.% (0.28 at%) at 450 °C. Therefore, the maximum predicted solid solution strengthening effect of Cu at room temperature calculated as $\sigma_{SS} = 57.2 C_{Cu}$ [57] is decreased from 16 MPa for the samples pre-treated at 450 °C to 11 MPa for the samples pre-treated at 300 °C. Strengthening effect for the samples pre-treated at 300–350 °C, as well as strength at 200–300 °C, was the result of cooperative effect of the *I*-phase and θ' precipitates. Meanwhile, the expected strengthening effect of the θ' -phase is weak due to a low solute Cu and related low number density of θ' -phase for the studied alloy and comparatively coarse θ' precipitates.

In the studied Al-Cu-Mn alloy, the *I*-phase precipitates near dislocations heterogeneously (Figure 6b). Heterogeneous nucleation of the *I*-phase was observed for Al-Mn-Mg alloys and pre-straining significantly increased the number density of precipitates [25,58]. Further investigations should be focused to study the influence of a low temperature thermomechanical treatment on the *I*-phase precipitates parameters and properties of the Al-Cu-Mn-based alloys. Pre-straining before aging at a temperature of 300 °C should increase the fraction of the fine *I*-phase precipitates, improve strengthening effect and strength properties of the alloys.

4. Summary

The precipitation behavior and mechanical properties at room temperature and 300 °C after ageing treatment in a temperature range of 300–400 °C for 3–148 h for as-cast Al-2%Mn-2%Cu alloy were studied.

According to XRD and microstructural studies, the alloy exhibited (Al) solid solution containing 1.7 ± 0.2 Mn wt%, $\text{Al}_{20}\text{Cu}_2\text{Mn}_3$, Al_2Cu , and Al_6Mn phases of solidification origin in as-cast state. The maximum hardening effect was revealed after aging of as-cast alloy at 300 °C for a time above 148 h, at 350 °C for 48 h, and at 400 °C for 32 h. The θ' -phase with a high size stability precipitated in a temperature range of 300–350 °C, and additionally, the *I*-phase precipitates with a mean size in a range of 30–50 nm were observed after long-term aging at 300 °C for 148 h and after 350 °C for 8–48 h. The structure of precipitates changed from the quasicrystalline to the crystalline with the formation of the orthorhombic *T*-phase precipitates during aging at temperature of 400 °C. The aging of as-cast samples in a temperature range of 300–400 °C provided a higher yield strength at room temperature compared to that of for 450 °C. A long-term aging at 300 °C provided an increased yield strength values at elevated compression temperature.

Author Contributions: Conceptualization, A.V.M.; methodology, N.Y.T.; software, A.D.K.; validation, A.D.K.; formal analysis, A.M.; investigation, A.M., A.V.M. and A.S.P.; resources, A.S.P.; data curation, A.M.; writing—original draft preparation, A.V.M.; writing—review and editing, A.G.M. and A.V.M.; visualization, A.V.M.; supervision, A.V.M.; project administration, A.V.M.; funding acquisition, A.V.M. All authors have read and agreed to the published version of the manuscript.

Funding: Hardness evolution, electrical resistance, and TEM studies was funded by RFBR, project No. 20-03-00778. Compression tests and XRD data were funded by RSF in a framework of Grant No. 21-79-00273. TEM study was performed in Collective Use Equipment Center “Materials Science and Metallurgy” working due to financial support of equipment modernization represented by the Ministry of Higher Education and Science of Russian Federation (No. 075-15-2021-696).

Institutional Review Board Statement: Not applicable.

Informed Consent Statement: Not applicable.

Data Availability Statement: The data presented in this study are available on request from the corresponding author.

Acknowledgments: The authors thank the members of the scientific school NSh-1752.2022.4 for discussing the results and SEM studies.

Conflicts of Interest: The authors declare no conflict of interest.

References

1. Korotkova, N.O.; Shurkin, P.K.; Cherkasov, S.O.; Aksenov, A.A. Effect of Copper Concentration and Annealing Temperature on the Structure and Mechanical Properties of Ingots and Cold-Rolled Sheets of Al-2% Mn Alloy. *Russ. J. Non-Ferrous Met.* **2022**, *63*, 190–200. [[CrossRef](#)]
2. Belov, N.A.; Akopyan, T.K.; Korotkova, N.O.; Shurkin, P.K.; Timofeev, V.N.; Raznitsyn, O.A.; Sviridova, T.A. Structure and heat resistance of high strength Al-3.3%Cu-2.5%Mn-0.5%Zr (wt%) conductive wire alloy manufactured by electromagnetic casting. *J. Alloys Compd.* **2022**, *891*, 161948. [[CrossRef](#)]
3. Dar, S.M.; Liao, H.; Xu, A. Effect of Cu and Mn content on solidification microstructure, *T*-phase formation and mechanical property of Al Cu Mn alloys. *J. Alloys Compd.* **2019**, *774*, 758–767. [[CrossRef](#)]
4. Belov, N.A.; Akopyan, T.K.; Korotkova, N.O.; Cherkasov, S.O.; Yakovleva, A.O. Effect of Fe and Si on the Phase Composition and Microstructure Evolution in Al-2 wt.% Cu-2 wt.% Mn Alloy During Solidification, Cold Rolling and Annealing. *JOM* **2021**, *73*, 3827–3837. [[CrossRef](#)]
5. SAmer, M.; Barkov, R.Y.; Prosviryakov, A.S.; Pozdnyakov, A.V. Structure and Properties of New Heat-Resistant Cast Alloys Based on the Al-Cu-Y and Al-Cu-Er Systems. *Phys. Met. Metallogr.* **2021**, *122*, 908–914. [[CrossRef](#)]
6. Belov, N.A.; Korotkova, N.O.; Shurkin, P.K.; Aksenov, A.A. Substantiation of the Copper Concentration in Thermally Stable Wrought Aluminum Alloys Containing 2 wt % of Mn. *Phys. Met. Metallogr.* **2020**, *121*, 1211–1219. [[CrossRef](#)]
7. Meng, F.; Wang, Z.; Zhao, Y.; Zhang, D.; Zhang, W. Microstructures and Properties Evolution of Al-Cu-Mn Alloy with Addition of Vanadium. *Metals* **2016**, *7*, 10. [[CrossRef](#)]

8. Shen, Z.; Liu, C.; Ding, Q.; Wang, S.; Wei, X.; Chen, L.; Li, J.; Zhang, Z. The structure determination of $\text{Al}_{20}\text{Cu}_2\text{Mn}_3$ by near atomic resolution chemical mapping. *J. Alloys Compd.* **2014**, *601*, 25–30. [[CrossRef](#)]
9. Shuncai, W.; Chunzhi, L.; Minggao, Y. Determination of structure of $\text{Al}_{20}\text{Cu}_2\text{Mn}_3$ phase in Al-Cu-Mn alloys. *Mater. Res. Bull.* **1989**, *24*, 1267–1270. [[CrossRef](#)]
10. Zhang, W.; Lin, B.; Fan, J.; Zhang, D.; Li, Y. Microstructures and mechanical properties of heat-treated Al–5.0Cu–0.5Fe squeeze cast alloys with different Mn/Fe ratio. *Mater. Sci. Eng. A* **2013**, *588*, 366–375. [[CrossRef](#)]
11. Gao, Y.H.; Cao, L.F.; Yang, C.; Zhang, J.Y.; Liu, G.; Sun, J. Co-stabilization of θ' - Al_2Cu and Al_3Sc precipitates in Sc-microalloyed Al–Cu alloy with enhanced creep resistance. *Mater. Today Nano* **2019**, *6*, 100035. [[CrossRef](#)]
12. Poplawsky, J.D.; Milligan, B.K.; Allard, L.F.; Shin, D.; Shower, P.; Chisholm, M.F.; Shyam, A. The synergistic role of Mn and Zr/Ti in producing θ' /L12 co-precipitates in Al–Cu alloys. *Acta Mater.* **2020**, *194*, 577–586. [[CrossRef](#)]
13. Shyam, A.; Roy, S.; Shin, D.; Poplawsky, J.D.; Allard, L.F.; Yamamoto, Y.; Morris, J.R.; Mazumder, B.; Idrobo, J.C.; Rodriguez, A.; et al. Elevated temperature microstructural stability in cast AlCuMnZr alloys through solute segregation. *Mater. Sci. Eng. A* **2019**, *765*, 138279. [[CrossRef](#)]
14. Gwalani, B.; Liu, J.; Lambeets, S.; Olszta, M.; Poplawsky, J.; Shyam, A.; Devaraj, A. Rapid assessment of interfacial stabilization mechanisms of metastable precipitates to accelerate high-temperature Al-alloy development. *Mater. Res. Lett.* **2022**, *10*, 771–779. [[CrossRef](#)]
15. Bahl, S.; Rakhmonov, J.U.; Kenel, C.; Dunand, D.C.; Shyam, A. Effect of grain-boundary θ - Al_2Cu precipitates on tensile and compressive creep properties of cast Al–Cu–Mn–Zr alloys. *Mater. Sci. Eng. A* **2022**, *840*, 142946. [[CrossRef](#)]
16. Michi, R.A.; Bahl, S.; Fancher, C.M.; Sisco, K.; Allard, L.F.; An, K.; Yu, D.; Dehoff, R.R.; Plotkowski, A.; Shyam, A. Load shuffling during creep deformation of an additively manufactured AlCuMnZr alloy. *Acta Mater.* **2023**, *244*, 118557. [[CrossRef](#)]
17. Cai, Z.; Liu, H.; Wang, R.; Peng, C.; Feng, Y.; Wang, X. Microstructure and Mechanical Properties of the Extruded Al–Cu–Mn–Sc–Zr Alloy during Single-Stage and Two-Stage Aging. *J. Mater. Eng. Perform.* **2022**, *32*, 185–198. [[CrossRef](#)]
18. Belov, N.A.; Akopyan, T.K.; Shurkin, P.K.; Korotkova, N.O. Comparative analysis of structure evolution and thermal stability of commercial AA2219 and model Al-2 wt%Mn-2 wt%Cu cold rolled alloys. *J. Alloys Compd.* **2021**, *864*, 158823. [[CrossRef](#)]
19. Amer, S.M.; Mamzurina, O.I.; Loginova, I.S.; Glavatskikh, M.V.; Barkov, R.Y.; Pozdniakov, A.V. Effect of Mn Addition on the Phase Composition and Strengthening Behavior of AlCuYbZr and AlCuGdZr Alloys. *JOM* **2022**, *74*, 3646–3654. [[CrossRef](#)]
20. Chen, W.; Zhang, W.; Ding, D.; Xiao, D. Microstructure of Al-5Cu-1Li-0.6Mg-0.5Ag-0.5Mn Alloys. *Metals* **2020**, *11*, 37. [[CrossRef](#)]
21. Zupanič, F.; Wang, D.; Gspan, C.; Bončina, T. Precipitates in a quasicrystal-strengthened Al–Mn–Be–Cu alloy. *Mater. Charact.* **2015**, *106*, 93–99. [[CrossRef](#)]
22. Bončina, T.; Albu, M.; Zupanič, F. Ageing of Al–Mn–Cu–Be Alloys for Stimulating Precipitation of Icosahedral Quasicrystals. *Metals* **2020**, *10*, 937. [[CrossRef](#)]
23. Bončina, T.; Zupanič, F. In situ TEM study of precipitation in a quasicrystal-strengthened AL-alloy. *Arch. Metall. Mater.* **2017**, *62*, 5–9. [[CrossRef](#)]
24. Mochugovskiy, A.; Tabachkova, N.; Mikhaylovskaya, A. Annealing induced precipitation of nanoscale icosahedral quasicrystals in aluminum based alloy. *Mater. Lett.* **2019**, *247*, 200–203. [[CrossRef](#)]
25. Mochugovskiy, A.G.; Tabachkova, N.Y.; Mikhaylovskaya, A.V. Nanodispersoids of the quasicrystalline I-phase in Mn- and Mg-bearing aluminum-based alloys. *Mater. Lett.* **2021**, *284*, 128945. [[CrossRef](#)]
26. Mochugovskiy, A.G.; Barkov, R.Y.; Mikhaylovskaya, A.V.; Loginova, I.S.; Yakovtseva, O.A.; Pozdniakov, A.V. Structure and Properties of Al–4.5Mg–0.15Zr Compositions Alloyed with Er, Y, and Yb. *Phys. Met. Metallogr.* **2022**, *123*, 466–473. [[CrossRef](#)]
27. Mikhaylovskaya, A.V.; Kishchik, A.A.; Kotov, A.D.; Rofman, O.V.; Tabachkova, N.Y. Precipitation behavior and high strain rate superplasticity in a novel fine-grained aluminum based alloy. *Mater. Sci. Eng. A* **2019**, *760*, 37–46. [[CrossRef](#)]
28. Macerl, M.; Zupanič, F.; Hočurščak, L.; Klobčar, D.; Kovács, A.; Bončina, T. Microstructure and Properties after Friction Stir Processing of Twin-Roll Cast Al–Mn–Cu–Be Alloy. *Crystals* **2022**, *12*, 630. [[CrossRef](#)]
29. Chen, R.; Wang, H.; Sun, Z.; He, B. Study of icosahedral quasi-crystalline phase $\text{T}_2\text{-Al}_6\text{CuLi}_3$ and transformation in 2A97 Al–Li alloy fabricated by laser additive manufacturing. *Mater. Lett.* **2022**, *316*, 132014. [[CrossRef](#)]
30. Zupanič, F.; Gspan, C.; Burja, J.; Bončina, T. Quasicrystalline and L12 precipitates in a microalloyed Al–Mn–Cu alloy. *Mater. Today Commun.* **2020**, *22*, 100809. [[CrossRef](#)]
31. Mikhaylovskaya, A.V.; Kishchik, A.A.; Tabachkova, N.Y.; Prosviryakov, A.S.; Mochugovskiy, A.G. Influence of Secondary Quasicrystalline I-Phase Precipitates on the Grain Structure and Mechanical Properties of the Al–Mg–Mn Alloy. *Phys. Met. Metallogr.* **2022**, *123*, 474–481. [[CrossRef](#)]
32. Mochugovskiy, A.G.; Tabachkova, N.Y.; Ghayoumabadi, M.E.; Cheverikin, V.V.; Mikhaylovskaya, A.V. Joint effect of quasicrystalline icosahedral and L12-structured phases precipitation on the grain structure and mechanical properties of aluminum-based alloys. *J. Mater. Sci. Technol.* **2021**, *87*, 196–206. [[CrossRef](#)]
33. Afifi, M.A.; Wang, Y.C.; Pereira, P.H.; Wang, Y.; Li, S.; Huang, Y.; Langdon, T.G. Characterization of precipitates in an Al–Zn–Mg alloy processed by ECAP and subsequent annealing. *Mater. Sci. Eng. A* **2018**, *712*, 146–156. [[CrossRef](#)]
34. Stan-Głowińska, K.; Lityńska-Dobrzyńska, L.; Rogal, Ł. Influence of Fe addition on the formation of a quasicrystalline phase in bulk Al-rich Al Mn base alloys. *Mater. Charact.* **2017**, *128*, 203–208. [[CrossRef](#)]

35. Stan-Głowińska, K.; Lityńska-Dobrzyńska, L.; Kania, B.; Dutkiewicz, J.; Rogal, Ł.; Skuza, W.; Wojewoda-Budka, J.; Gordillo, M.A.; Wiezorek, J.M. Effects of hot-compaction on the structure and properties of Al-Mn-Fe-X alloys strengthened with quasi-crystalline icosahedral phase. *Mater. Des.* **2017**, *126*, 162–173. [[CrossRef](#)]
36. Stan-Głowińska, K.; Rogal, Ł.; Góral, A.; Wierzbicka-Miernik, A.; Wojewoda-Budka, J.; Schell, N.; Lityńska-Dobrzyńska, L. Formation of a quasicrystalline phase in Al–Mn base alloys cast at intermediate cooling rates. *J. Mater. Sci.* **2017**, *52*, 7794–7807. [[CrossRef](#)]
37. Wolf, W.; Bolfarini, C.; Kiminami, C.S.; Botta, W.J. Fabrication of Al-matrix composite reinforced with quasicrystals using conventional metallurgical fabrication methods. *Scr. Mater.* **2019**, *173*, 21–25. [[CrossRef](#)]
38. Wolf, W.; Bolfarini, C.; Kiminami, C.S.; Botta, W.J. Designing new quasicrystalline compositions in Al-based alloys. *J. Alloys Compd.* **2020**, *823*, 153765. [[CrossRef](#)]
39. Chen, Z.; Zhang, Q.; Dong, B.; Liu, Z. Microstructure and Thermal Stability of Icosahedral Quasicrystals in Suction Casting Al-6 at.%Mn(–2 at.%Be) Alloys. *J. Mater. Eng. Perform.* **2020**, *29*, 447–455. [[CrossRef](#)]
40. Rozman, N.; Medved, J.; Zupanič, F. Microstructural evolution in Al–Mn–Cu–(Be) alloys. *Philos. Mag.* **2011**, *91*, 4230–4246. [[CrossRef](#)]
41. Leskovar, B.; Samardžija, Z.; Koblar, M.; Naglič, I.; Markoli, B. Development of an Al-Mn-Si-Based Alloy with an Improved Quasicrystalline-Forming Ability. *JOM* **2020**, *72*, 1533–1539. [[CrossRef](#)]
42. Zupanič, F.; Bončina, T. Heat-Resistant Al-Alloys with Quasicrystalline and L12- Precipitates. *Solid State Phenom.* **2022**, *327*, 26–32. [[CrossRef](#)]
43. Belov, N.A.; Eskin, D.G.; Aksenov, A.A. *Multicomponent Phase Diagrams: Applications for Commercial Aluminum Alloys*; Elsevier: London, UK, 2005. [[CrossRef](#)]
44. *Casting Aluminum Alloys*; Elsevier: London, UK, 2019. [[CrossRef](#)]
45. Milligan, B.; Ma, D.; Allard, L.; Clarke, A.; Shyam, A. Dislocation- θ' (Al₂Cu) interactions during creep deformation of an Al-Cu alloy. *Scr. Mater.* **2022**, *217*, 114739. [[CrossRef](#)]
46. Rakhmonov, J.; Liu, K.; Chen, G.X. Effects of Compositional Variation on the Thermal Stability of θ' -Al₂Cu Precipitates and Elevated-Temperature Strengths in Al-Cu 206 Alloys. *J. Mater. Eng. Perform.* **2020**, *29*, 7221–7230. [[CrossRef](#)]
47. Yin, Q.; Chen, G.; Shu, X.; Zhang, B.; Li, C.; Dong, Z.; Cao, J.; An, R.; Huang, Y. Analysis of interaction between dislocation and interface of aluminum matrix/second phase from electronic behavior. *J. Mater. Sci. Technol.* **2023**, *136*, 78–90. [[CrossRef](#)]
48. Dai, H.; Wang, L.; Dong, B.; Miao, J.; Lin, S.; Chen, H. Microstructure and high-temperature mechanical properties of new-type heat-resisting aluminum alloy Al_{6.5}Cu₂Ni_{0.5}Zr_{0.3}Ti_{0.25}V under the T7 condition. *Mater. Lett.* **2023**, *332*, 133503. [[CrossRef](#)]
49. Bello, N.; Larignon, C.; Douin, J. Long-term thermal ageing of the 2219-T851 and the 2050-T84 Al-Cu alloys. *Mater. Today Commun.* **2021**, *29*, 102834. [[CrossRef](#)]
50. Dong, X.; Guo, Y.; Wang, J.; Xia, F.; Ma, K.; Duan, H.; Yang, Z.; Wang, P.; Liang, M.; Li, J. Novel AlCu solute cluster precipitates in the Al–Cu alloy by elevated aging and the effect on the tensile properties. *Mater. Sci. Eng. A* **2023**, *862*, 144454. [[CrossRef](#)]
51. Li, X.Z.; Kuo, K.H. Orthorhombic crystalline approximants of the Al-Mn-Cu decagonal quasicrystal. *Philos. Mag. B* **1992**, *66*, 117–124. [[CrossRef](#)]
52. Wang, J.; Zhang, B.; He, Z.B.; Wu, B.; Ma, X.L. Atomic-scale mapping of twins and relevant defective structures in Al₂₀Cu₂Mn₃ decagonal approximant. *Philos. Mag.* **2016**, *96*, 2457–2467. [[CrossRef](#)]
53. Chen, Y.Q.; Pan, S.P.; Zhu, B.X.; Liu, X.; Liu, W.H.; Tang, S.W. The evolution of orientation relationships during the transformation of a twin-free T-particle to tenfold T-twins in an Al alloy during homogenisation. *Mater. Charact.* **2018**, *141*, 59–73. [[CrossRef](#)]
54. Chen, Y.Q.; Pan, S.P.; Liu, W.H.; Liu, X.; Tang, C.P. Morphologies, orientation relationships, and evolution of the T-phase in an Al-Cu-Mg-Mn alloy during homogenisation. *J. Alloys Compd.* **2017**, *709*, 213–226. [[CrossRef](#)]
55. Chen, Y.Q.; Tang, Z.H.; Pan, S.P.; Liu, W.H.; Song, Y.F.; Liu, Y.; Zhu, B.W.; Zhou, W.; Shen, F.H. A new type of anti-phase boundaries in the T(Al₂₀Cu₂Mn₃) phase and the pre-deformation effect on T phase precipitation. *Intermetallics* **2020**, *127*, 106977. [[CrossRef](#)]
56. Geng, J.; Li, Y.; Liu, G.; Xiao, H.; Hong, T.; Huang, J.; Wang, M.; Chen, D.; Wang, H. Segregation of S precipitates at T/Al interfaces and relevant effects on localized corrosion mechanisms in Al-Cu-Mg alloy. *Mater. Charact.* **2020**, *168*, 110571. [[CrossRef](#)]
57. Zolotarevsky, N.Y.; Solonin, A.N.; Churyumov, A.Y.; Zolotarevsky, V.S. Study of work hardening of quenched and naturally aged Al–Mg and Al–Cu alloys. *Mater. Sci. Eng. A* **2009**, *502*, 111–117. [[CrossRef](#)]
58. Mochugovskiy, A.G.; Mukhamejanova, A.B.; Kotov, A.D.; Yakovtseva, O.A.; Tabachkova, N.Y.; Mikhaylovskaya, A.V. The effect of pre-straining on the annealing-induced precipitation behavior of the icosahedral I-phase in an aluminum-based alloy. *Mater. Lett.* **2022**, *310*, 131517. [[CrossRef](#)]

Disclaimer/Publisher’s Note: The statements, opinions and data contained in all publications are solely those of the individual author(s) and contributor(s) and not of MDPI and/or the editor(s). MDPI and/or the editor(s) disclaim responsibility for any injury to people or property resulting from any ideas, methods, instructions or products referred to in the content.